

# Structure Optimization and Exergy Analysis of a Two-stage TEC with Two Different Connections

Henan Sun<sup>a</sup>, Sergio Usón Gil<sup>b</sup>, Wei Liu<sup>a</sup>, Zhichun Liu<sup>a,\*</sup>

<sup>a</sup>School of Energy and Power Engineering, Huazhong University of Science and  
Technology, Wuhan 430074, China

<sup>b</sup>Department of Mechanical Engineering. CIRCE Institute, University of Zaragoza,  
Zaragoza, Spain

\*Corresponding author. Tel 027-87542618, E-mail: [zcliu@hust.edu.cn](mailto:zcliu@hust.edu.cn)

## Abstract

This paper develops three dimensional numerical models of a two-stage series-connected TEC model and a two-stage parallel-connected TEC model. NSGA-II is used to optimize their electric current, height of lower stage and ratio of channel width and thickness of fin in the case of constant thermoelectric material volume. Two objectives, exergy efficiency and irreversibility are considered simultaneously. The optimal values one Pareto front are obtained by three decision making methods, Shannon's entropy, TOPSIS and LINMAP, while deviation index is a criterion for evaluating three decision making methods. Sensitive analysis has been carried out to investigate the influence of three variables to be optimized. And TEC with and without plate-fin heat exchanger have been compared. The results show that solution selected by LINMAP is the most compromising solution. The parallel connected TEC saves about 50% of the power consumption compared to the series connected TEC under the same temperature difference. Optimal variables are discussed to obtain the most energy efficient solution with optimal configuration and plate-fin heat exchanger.

**Keywords:** Thermoelectric cooler; Structure Optimization; Exergy Analysis; Multi-objective; Irreversibility

## 1. Introduction

Thermoelectric cooler (TEC) has been widely used in various electronic applications to dissipate heat ranging from milliwatts to several watts for its steady,

1 compact volume, non-pollution, noiseless, safe and reliable, and long service life [1].  
2 Thermoelectric cooler convert the electricity directly to the cooling power, and it can  
3 achieve high precision temperature control through control of the electrical current.  
4 TEC is used in information technology, such as infrared detectors, lasers, and  
5 computer chips. It is used in medicine in semiconductor refrigeration and transporting  
6 blood vessels, cold packers, cryo-microtome, ventilators, and PCR machines. Another  
7 occasion that may have practical application significance for thermoelectric materials  
8 is to provide a cryogenic environment for the use of superconducting materials.  
9

10 The principle of thermoelectric cooling is Peltier effect which absorbs or releases  
11 heat at the junction when electrical current applied and different conductors are  
12 employed in a closed circuit. Now, commercially produced single-stage TEC can  
13 achieve approximately 70 K temperature difference between cold side and hot side  
14 given that the hot side remains the ambient temperature [2]. But the defects that the  
15 comparable high unit cost and relative low efficiency in refrigeration cannot be  
16 ignored either. Some studies make improvements to thermoelectric materials  
17 technology, increase its figure of merit (ZT value) from the intrinsic properties of  
18 thermoelectric materials. Ways in which this may be realized include a reduction in  
19 the thermal conductivity of the lattice, improved thermostability through doping,  
20 removal of impurities, and improved microstructure design [3-11]. Another approach  
21 is to optimize the geometric configurations. A lot of studies investigated the  
22 configuration of TEC and its influence to TEC's performance [12-14]. Cheng YH et al.  
23 [15] optimized the leg length, leg area and number of legs of TEC in a confined  
24 volume to maximize the cooling capacity in the constraint of minimum COP and  
25 maximum cost, their results showed that the TEC can reach its maximum cooling  
26 power even in different electrical current, with increase of electrical current, leg area  
27 increase and the number of legs decrease to meet its optimize geometry configuration.  
28 And they also compared two-stage TECs with single electric-source and dual  
29 electric-source, and the effect of joint thermal resistance was also studied in this paper  
30 [16]. Chen JH et al. further studied the multi-objective optimization for both COP and  
31 cooling power, and they found there is an optimum leg length ratio when two stages  
32  
33  
34  
35  
36  
37  
38  
39  
40  
41  
42  
43  
44  
45  
46  
47  
48  
49  
50  
51  
52  
53  
54  
55  
56  
57  
58  
59  
60  
61  
62  
63  
64  
65

1 current are given, and they also studied on the influence of thickness of ceramic  
2 substrate on TEC's performance [17].  
3

4 Exergy analysis is also studied to identify the irreversibility at each part of the  
5 TEC system. Sudhanshu S et al. [18] introduced the relationships between exergy,  
6 irreversibility, entropy generation rate and second law efficiency of single- and multi-  
7 stage TEC systematically. Siamak J et al. [19] proposed a novel integration of  
8 trans-critical CO<sub>2</sub> refrigeration cycle with TEC and TEG modules in gas cooler and  
9 sub-cooler, TEG produces power from waste heat in gas cooler and offers the power  
10 to TEC to sub-cool the refrigerant. They investigate the relationship between the  
11 performance (exergetic efficiency, COP) and system parameter (pressure and  
12 temperature). The results shows that the integration system improve the COP about 19%  
13 compare with simple cycle, Ranjana A [20] investigated single -stage, two-stage  
14 parallel and series thermoelectric heat pump, ecological function, COP and heating  
15 load were optimized simultaneously, Shannon's entropy, Fuzzy Bellman - Zadeh, and  
16 TOPSIS were adopt as decision making method to choose a reasonable solution for  
17 performance of thermoelectric heat pump. Zhu L et al. [21] combined TEC with a  
18 plate-fin heat exchanger, the entropy generation rate of cooled object, TEC and fin as  
19 well as second law efficiency were analyzed in the paper, the results show the entropy  
20 generation rate increases with the increase of electrical current, while the temperature  
21 difference increase with the increase of the number of transfer units (NTU). Meng F et  
22 al. [22] established a TEC with finned heat exchanger, single-factor sensible analysis  
23 and first and second thermodynamic analysis were conducted as well, the results  
24 showed that the heat exchanger fin-base area has the greatest effect on the TEC's  
25 performance, when the fin-base area is 3 times as large as the substrate area, it is both  
26 commercial and close to performance limits. S Manikandan [23] proposed four types  
27 of thermodynamic TEC, which respectively are reversible, endoreversible,  
28 exoreversible and irreversible model, completed the detail of exergy and  
29 irreversibility of them and discussed the influence of substrate area and contact  
30 resistance to TEC's performance, for irreversible model, the hot junction temperature  
31 is higher than heat sink temperature while the cold junction temperature is lower than  
32  
33  
34  
35  
36  
37  
38  
39  
40  
41  
42  
43  
44  
45  
46  
47  
48  
49  
50  
51  
52  
53  
54  
55  
56  
57  
58  
59  
60  
61  
62  
63  
64  
65

1 heat source temperature. They also conducted exergy analysis on four thermodynamic  
2 models of thermoelectric heat pump [24], the results shows that in thermoelectric heat  
3 pump, exergy efficiency always lower than energy efficiency and it increases with  
4 increase of temperature difference. The effect of internal irreversibilities in the  
5 performance of the thermoelectric heat pump is more when compared with the  
6 external irreversibilities. Manikandan et al. [25] introduce a novel annular  
7 thermoelectric cooler (ATEC), they build an exoreversible model, the effect of shape  
8 parameter, temperature difference and electrical contact resistance on its performance  
9 (exergy/energy efficiency, COP) have been studied and impact of Thomson effect on  
10 its performance has been studied too, the results show that the performance of annular  
11 TEC is lower than the flat plate TEC and Thomson effect has considerably increase  
12 the exergy and energy efficiency of annular TEC. Kaushik SC [26] investigated the  
13 influence of Thomson effect on TEC's performance, the results showed that Thomson  
14 effect has positive effect on cooling power and efficiency; the internal irreversibilities  
15 is larger than external irreversibilities numerically; they also found that for optimum  
16 cooling power, the ratio of thermocouples of hotter stage and colder stage  
17 approximately equals to 2, because according to energy balance, the hotter junction  
18 not only dissipate heat from the cold junction but also the Joule heat generated by  
19 thermoelectric materials and copper interconnectors. Arash N et al. [27] analysis a  
20 two-stage cascaded TEC in exergy and exergoeconomic performance, and effect of  
21 geometry parameters on its performance.

22 Referring to the above literature, previous multi-level TEC studies were conducted  
23 with electrical insulation between the stages, whereas the present study is focus on the  
24 comparison between series connection between stages and parallel connection  
25 between stages. A two-stage series-connected TEC model combining with a fin heat  
26 exchanger comparing with a two-stage parallel-connected TEC is studied. The  
27 irreversible model with negligible of contact resistance of both series connected TEC  
28 and parallel connected TEC are built. According to literature [23], one pair of  
29 thermocouples is set at the colder stage and two pairs of thermocouples are set at the  
30 hotter stage. While the assumption of fixed wall temperature condition at the hot side  
31  
32  
33  
34  
35  
36  
37  
38  
39  
40  
41  
42  
43  
44  
45  
46  
47  
48  
49  
50  
51  
52  
53  
54  
55  
56  
57  
58  
59  
60  
61  
62  
63  
64  
65

is impractical, since the hot side dissipates heat to the environment, and the temperature of hot-side substrate is varying with heat release, so in this paper, a fixed heat source temperature and a fixed air temperature at the inlet of the fin are applied in the series and parallel models. Since electrical current significantly affect the COP and cooling power of TEC; changing the TE legs' height may causes a change in the resistance value of TE legs; and relative width of the channel of fin heat exchanger can affect the convection heat. So electrical current, the lower height of TE legs (Assumed that the total height of two stage TE legs is fixed) and the ratio of the channel width to thickness of fin are optimized to obtain its optimum thermodynamic performance.

## 2. Modeling

### 2.1. Two-stage series-connected TEC model

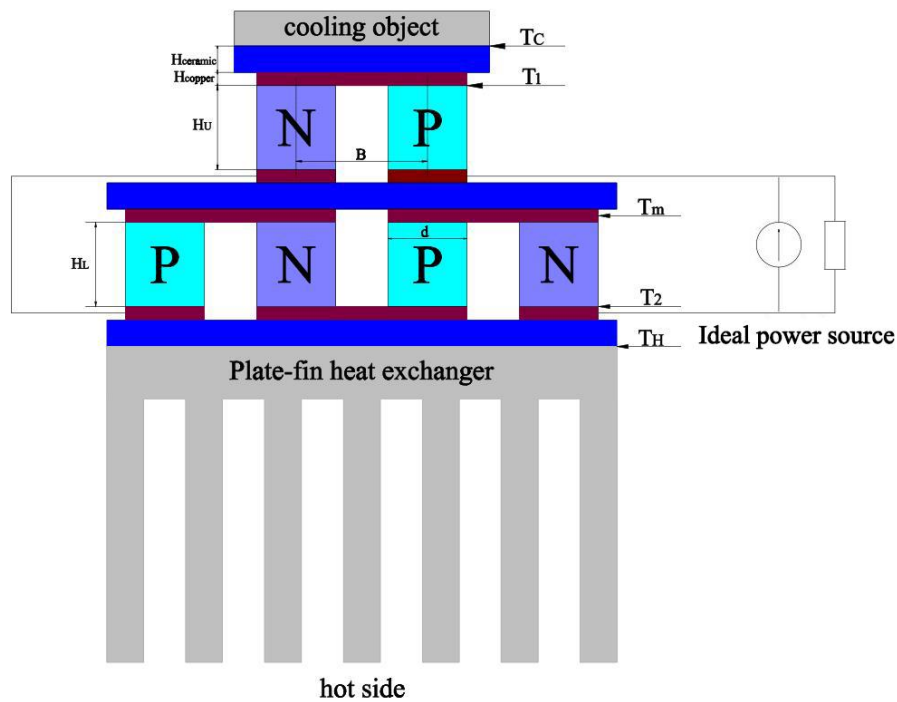


Fig. 1. Schematic diagram of the two-stage series-connected TEC system.

Fig.1 shows the schematic diagram of the two-stage series-connected TEC system. The TEC system consists of three pairs of cylindrical thermoelectric couples---one pair for the colder stage and two pairs for the hot stage, a plate-fin heat exchanger on the cold side, electrical isolated  $Al_2O_3$  ceramic, copper interconnectors, an ideal power

source to supply constant current to TEC and several electric wires. We should notice that the ideal power source is equivalent to an electrical current source with an infinite resistance connected in parallel. The thermoelectric cooler is sandwiched between the cooling object and the plate-fin heat exchanger. The specific parameters of the TEC model are listed in Table 1.

Table 1 Geometric parameters of TEC

Parameter	Symbol	Value	Unit
Thickness of the substrate	$H_{ceramic}$	0.5	mm
Thickness of interconnector	$H_{copper}$	0.25	mm
Total height of TE legs	$H$	3.2	mm
Diameter of TE legs	$d$	1.5	mm
Distance between N- and P-type TE leg	$B$	2.5	mm
Cold side substrate of TEC	$A_C$	4.85×2.33	mm <sup>2</sup>
Hot side substrate of TEC	$A_H$	9.7×2.33	mm <sup>2</sup>
Variables	Symbol	Value	Unit
Electric current	$I$		A
Height of the lower TE legs	$H_L$		mm

Thermoelectric material plays a main role in thermoelectric device, the ability of a given material to efficiently produce thermoelectric power is related to its dimensionless figure of merit, also called ZT value [2]. It is calculated as:  $ZT = \alpha^2 \sigma T / \lambda$ , where  $\alpha$  is Seebeck coefficient (V/K),  $\sigma$  is electrical conductivity (S/m), T is absolute temperature (K), and  $\lambda$  is thermal conductivity (W/m·K). For good efficiency, materials with high electrical conductivity, low thermal conductivity and high Seebeck coefficient are needed. And since the Seebeck coefficient, the electrical conductivity and the thermal conductivity are temperature-sensitive, the ZT value also changes substantially with temperature. Bi<sub>2</sub>Te<sub>3</sub> is a thermoelectric material that has better performance when temperature is below 450 K, so it is selected as the thermoelectric material for the upper and lower stage TE legs. Table 2 lists all of the material properties, which can be approximated with polynomial expressions.

Table 2 The temperature-dependent material properties of TE legs

Material	Thermal conductivity [Wm <sup>-1</sup> K <sup>-1</sup> ]	Electrical conductivity [S/m]	Seebeck coefficient [V/K]
n-Bi <sub>2</sub> Te <sub>3</sub>	1.19E-05T <sup>2</sup> -0.005777T+2.00418	0.89631T <sup>2</sup> -860.754+262853.95	2.31E-09T <sup>2</sup> -1.65E-06T+6.89E-05
p-Bi <sub>2</sub> Te <sub>3</sub>	3.11E-05T <sup>2</sup> -0.02413T+5.90208	1.80184T <sup>2</sup> -2101.88T+686731.77	-1.30E-0910T <sup>2</sup> +1.17E-06T-8.80E-05

## 2.2. First law analysis of series-connected TEC model

Thermoelectric coolers operate by the Peltier effect. For a steady state multi-stage series-connected TEC, the absorbed heat on the cold side and the rejected heat on the hot side of two stages can be written as follows:

Colder stage:

$$Q_{C1} = m \left[ \alpha I T_1 - \frac{1}{2} I^2 R_1 - K(T_m - T_1) + \frac{\tau I(T_m - T_1)}{2} \right] \quad (1)$$

$$Q_{H1} = m \left[ \alpha I T_m + \frac{1}{2} I^2 R_1 - K(T_m - T_1) - \frac{\tau I(T_m - T_1)}{2} \right] \quad (2)$$

Hotter stage:

$$Q_{C2} = n \left[ \alpha I T_m - \frac{1}{2} I^2 R_2 - K(T_2 - T_m) + \frac{\tau I(T_2 - T_m)}{2} \right] \quad (3)$$

$$Q_{H2} = n \left[ \alpha I T_2 + \frac{1}{2} I^2 R_2 - K(T_2 - T_m) - \frac{\tau I(T_2 - T_m)}{2} \right] \quad (4)$$

Where  $m$  is the number of TE legs of colder stage (upper stage),  $n$  is the number of TE legs of hotter stage (lower stage), in this study,  $m$  and  $n$  are 1 and 2, respectively.  $\alpha$ ,  $K$ ,  $R$  and  $\tau$  are Seebeck coefficient, thermal conductivity, electrical resistance and Thomson coefficient respectively, which can be expressed as follow.  $I$  is electrical current supply.  $T_1$  and  $T_2$  are the temperature at the cold junction and hot junction of TEC, respectively.  $T_m$  is the temperature on the middle substrate.

$$\alpha = \overline{\alpha_p} - \overline{\alpha_n} \quad (5)$$

Where  $\overline{\alpha_p}$  and  $\overline{\alpha_n}$  are mean Seebeck coefficient of P and N type TE leg, and can be expressed as:

$$\overline{\alpha_p} = \frac{\int_{T_c}^{T_h} \alpha_p(T) dT}{T_h - T_c} \quad (6)$$

$$\overline{\alpha_n} = \frac{\int_{T_c}^{T_h} \alpha_n(T) dT}{T_h - T_c} \quad (7)$$

The thermal conductivity  $K$  is the sum of the thermal conductivity of P and N type, which can be expressed as:

$$K = \frac{\bar{\lambda}_p A_p}{L_p} + \frac{\bar{\lambda}_n A_n}{L_n} \quad (8)$$

Where  $\bar{\lambda}_p$  and  $\bar{\lambda}_n$  is the mean thermal conductivity of P and N type, which can be expressed as:

$$\bar{\lambda}_p = \frac{\int_{T_c}^{T_h} \lambda_p(T) dT}{T_h - T_c} \quad (9)$$

$$\bar{\lambda}_n = \frac{\int_{T_c}^{T_h} \lambda_n(T) dT}{T_h - T_c} \quad (10)$$

The electrical resistance of a thermoelectric pair can be expressed as:

$$R = R_p + R_n = \frac{L_p}{\bar{\sigma}_p A_p} + \frac{L_n}{\bar{\sigma}_n A_n} \quad (11)$$

Where  $\bar{\sigma}_p$  and  $\bar{\sigma}_n$  is mean electrical conductivity respectively, which can be expressed as:

$$\bar{\sigma}_p = \frac{\int_{T_c}^{T_h} \sigma_p(T) dT}{T_h - T_c} \quad (12)$$

$$\bar{\sigma}_n = \frac{\int_{T_c}^{T_h} \sigma_n(T) dT}{T_h - T_c} \quad (13)$$

Base on energy conservation law, the absorbed heat  $Q_{C1}$  transfer from the cooling object to the cold junction through the upper substrate, the rejected heat  $Q_{H2}$  transfer from the hot junction to the lower substrate. The balance equations are shown as follows:

$$Q_{C1} = U_C A_C (T_C - T_1) \quad (15)$$

$$Q_{H2} = U_H A_H (T_2 - T_H) \quad (16)$$

Combining the two equations above, the expression of  $T_1$  and  $T_2$  can be obtained:

$$T_1 = T_C - \frac{Q_{C1}}{U_C A_C} \quad (17)$$

$$T_2 = \frac{Q_{H2}}{U_H A_H} + T_H \quad (18)$$

Where  $U_C$  and  $U_H$  is the heat transfer coefficient of the  $Al_2O_3$  ceramic,  $A_C$  and  $A_H$  are the area of upper and lower substrate, respectively.  $T_H$  is the temperature of the hot side, and  $T_C$  is the temperature of the cold side. For cold side, in order to save computing resource, a fixed temperature on the cold side is set instead of a real cooling object, where  $T_C = 280.15 K$ . And the coefficient of performance (COP) of TEC can be expressed as:



$$COP = \frac{Q_{C1}}{Q_{H2} - Q_{C1}} \quad (19)$$

or

$$COP = \frac{Q_{C1}}{\text{Power}} \quad (20)$$

### 2.3. Two-stage parallel-connected TEC model

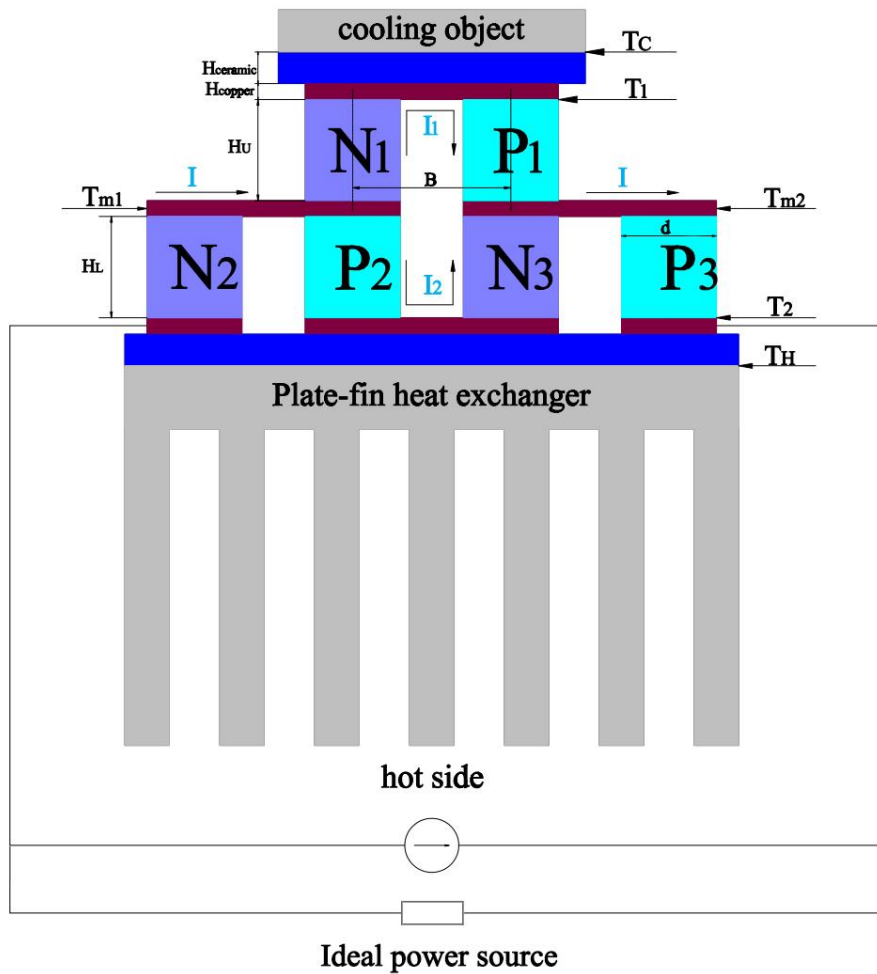


Fig. 2. Schematic diagram of the two-stage parallel-connected TEC system.

A two-stage parallel-connected TEC model is proposed to compare the performance with the series one. The schematic diagram of TEC model is shown in Fig. 2. The difference between two models is that an electrically insulated substrate is employed in the middle of series-connected TEC to impede the circuit connections

from lower stage to upper stage. But for parallel one, since the stages are both thermally and electrically conductive, there is no need for electrical insulation between the stages.

#### 2.4. First law analysis

For a steady state multi-stage parallel-connected TEC, the absorbed heat on the cold side and the rejected heat on the hot side of two stage can be written as follows, for express more intuitively, the three modules of the upper and lower stages are numbered 1, 2, 3 respectively, and the electrical current flow separately through the upper stage and the lower stage are  $I_1$  and  $I_2$ , respectively.

Colder stage:

$$Q_{C1} = (\alpha_{p1} - \alpha_{n1})I_1T_1 - \frac{1}{2}I_1^2(R_{p1} + R_{n1}) - K_{n1}(T_{m1} - T_1) - K_{p1}(T_{m2} - T_1) + \frac{1}{2}\tau_{p1}I_1(T_{m2} - T_1) - \frac{1}{2}\tau_{n1}I_1(T_{m1} - T_1) \quad (21)$$

$$Q_{H1} = \alpha_{p1}I_1T_{m2} - \alpha_{n1}I_1T_{m1} + \frac{1}{2}I_1^2(R_{p1} + R_{n1}) - K_{n1}(T_{m1} - T_1) - K_{p1}(T_{m2} - T_1) - \frac{1}{2}\tau_{p1}I_1(T_{m2} - T_1) + \frac{1}{2}\tau_{n1}I_1(T_{m1} - T_1) \quad (22)$$

Hotter stage:

$$Q_{C2} = (\alpha_{p2}I_2 - \alpha_{n2}I)T_{m1} - \frac{1}{2}I_2^2R_{p2} - \frac{1}{2}I^2R_{n2} - K_{p2}(T_2 - T_{m1}) - K_{n2}(T_2 - T_{m1}) + \frac{1}{2}(T_2 - T_{m1})(\tau_{p2}I_2 - \tau_{n2}I) + (\alpha_{p3}I - \alpha_{n3}I_2)T_{m2} - \frac{1}{2}I^2R_{p3} - \frac{1}{2}I_2^2R_{n3} - K_{p3}(T_2 - T_{m2}) - K_{n3}(T_2 - T_{m2}) + \frac{1}{2}\tau_{p3}I(T_2 - T_{m2}) - \frac{1}{2}\tau_{n3}I_2(T_2 - T_{m2}) \quad (23)$$

$$Q_{H2} = (\alpha_{p2}I_2 - \alpha_{n2}I)T_2 + \frac{1}{2}I_2^2R_{p2} + \frac{1}{2}I^2R_{n2} - K_{p2}(T_2 - T_{m1}) - K_{n2}(T_2 - T_{m1}) - \frac{1}{2}(T_2 - T_{m1})(\tau_{p2}I_2 - \tau_{n2}I) + (\alpha_{p3}I - \alpha_{n3}I_2)T_2 - \frac{1}{2}I^2R_{p3} + \frac{1}{2}I_2^2R_{n3} - K_{p3}(T_2 - T_{m2}) - K_{n3}(T_2 - T_{m2}) - \frac{1}{2}\tau_{p3}I(T_2 - T_{m2}) + \frac{1}{2}\tau_{n3}I_2(T_2 - T_{m2}) \quad (24)$$

It can be clearly seen that the heat rejected by  $N_1$  leg is absorbed by No.2 thermoelectric pair, and the heat rejected by  $P_1$  leg is absorbed by No.3 thermoelectric pair. According to energy-balance equation,  $T_1$  and  $T_2$  can be expressed as follows:

$$T_{m1} = \frac{I_2^2R_{p2} + I^2R_{n2} + 2K_{p2}T_2 + 2K_{n2}T_2 - \tau_{p2}T_2I_2 + \tau_{n2}T_2I + I_1^2R_{n1} + 2K_{n1}T_1 - \tau_{n1}T_1I_1}{2\alpha_{n1}I_1 + 2K_{n1} - \tau_{n1}I_1 - 2\alpha_{n2}I + 2\alpha_{p2}I_2 + 2K_{p2} + 2K_{n2} - \tau_{p2}I_2 + \tau_{n2}I} \quad (25)$$

$$T_{m2} = \frac{I_1^2 R_{p1} + 2K_{p1} T_1 + \tau_{p1} I_1 T_1 + I_2^2 R_{p3} + I_2^2 R_{n3} + 2K_{p3} T_2 + 2K_{n3} T_2 - \tau_{p3} I T_2 + \tau_{n3} I_2 T_2}{2K_{p1} + \tau_{p1} I_1 + 2\alpha_{p3} I - 2\alpha_{n3} I_2 - 2\alpha_{p1} I_1 + 2K_{p3} + 2K_{n3} - \tau_{p3} I + \tau_{n3} I_2} \quad (26)$$

## 2.5. Fin analysis

Since the small volume of the TEC model, there exists a problem of poor heat dissipation. The high operation temperature may cause the reduction of the life expectancy of the material and reduction of efficiency, so an effective method to enhance the heat transfer on the hot side of the TEC is important for improving operating performance. The hot side of the TEC model is cooled by a plate-fin, air works as the heat transfer fluid, it dissipates the heat produced by the TEC, Fig. 3 shows the configuration of the plate-fin, the length and width of fin is equals to those of lower substrate. The inlet air velocity  $U_0$  is 0.72 m/s, the inlet air temperature  $T_i'$  is 298.15 K. The thickness of the fin  $\delta_f$  equals to 0.4 mm, since the ratio of channel width and the thickness of fin ( $\gamma$ ) is variable, so the thickness of the fin can be determined by  $\gamma$ . Other geometric parameters are also listed in Table 3 [22].

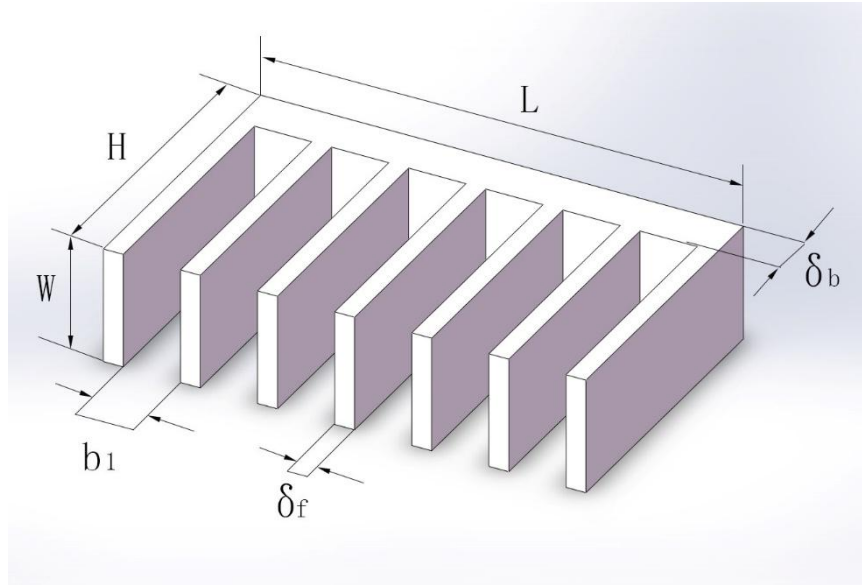


Fig. 3. Configuration of the plate-fin. Table 3 parameters of the plate-fin

Table 3 parameters of the plate-fin

Parameter	Symbol	Value	Unit
Thickness of the fin base	$\delta_b$	1	mm
Length of the fin	$H$	6	mm
Length of the fin base	$L$	9.7	mm
Width of the fin base	$W$	2.33	mm
Thickness of the fin	$\delta_f$	0.4	mm
Air velocity	$U_0$	0.72	m/s
inlet temperature	$T_f'$	298.15	K
Variables	Symbol	Value	Unit
Ratio of channel width to thickness of fin	$\gamma$		1
Channel width	$b_1$	$\gamma \times \delta_f$	mm
Number of the fin (in calculation)	NN	$(L + bs \times \delta_f) / (\delta_f + bs \times \delta_f)$	1
Number of the fin (integer)	N	Floor(NN)	1

### 3. Exergy analysis

Exergy analysis plays an important role in quantifying the quality of thermal energy from the perspective of technology use and economic value, in other words, it locates and quantifies the irreversibilities in the system[28-31]. In order to determine the percentage of the internal irreversibility and external irreversibility to total irreversibility, four different model have presented in literature [23], Reversible model (ideal), Endoreversible model, Exoreversible model and Irreversible model (actual). For thermoelectric material, it always has internal irreversibilities due to its intrinsic physical properties (low thermal conductivity, and Joule heat produced by internal electrical resistance), so Reversible model and Endoreversible model are incompatible with thermodynamic laws, while the irreversible model is the actual situation. So, exergy analysis of Irreversible model (actual) is discussed in this study.

For a steady state thermodynamic system, the exergy balance equation can be written as follows:

$$Ex_{in} = Ex_{out} + Ex_{lost} + Irr \quad (27)$$

Where  $Ex_{in}$  is the exergy input to the TEC system, since the electrical power supply is higher-quality energy than thermal energy, the electrical power supply is

100% exergy.  $Ex_{out}$  is the exergy output,  $Ex_{lost}$  is the exergy lost, and  $Irr$  is exergy destruction during the process.

The thermal exergy at the hot side which rejected heat to the fin base can be expressed as follows:

$$E_{Qh} = Q_h \left(1 - \frac{T_0}{T_h}\right) \quad (28)$$

And the thermal exergy at the cold side which absorbed heat from the cooling objective can be expressed as follows:

$$E_{Qc} = Q_c \left(\frac{T_0}{T_c} - 1\right) \quad (29)$$

For a two-stage TEC model, the exergy balance equation is shown as follows:

For colder stage

$$P_1 = Q_{c1} \left(\frac{T_0}{T_c} - 1\right) + Q_{H1} \left(1 - \frac{T_0}{T_m}\right) + Irr_1 \quad (30)$$

$$P_1 = Q_{H1} - Q_{c1} \quad (31)$$

Combine above two equations,

$$Irr_1 = T_0 \left(\frac{Q_{H1}}{T_m} - \frac{Q_{c1}}{T_c}\right) \quad (32)$$

Similar for hotter stage

$$P_2 = Q_{c2} \left(\frac{T_0}{T_m} - 1\right) + Q_{H2} \left(1 - \frac{T_0}{T_H}\right) + Irr_2 \quad (33)$$

$$P_2 = Q_{H2} - Q_{c2} \quad (34)$$

Combine the above two equations,

$$Irr_2 = T_0 \left(\frac{Q_{H2}}{T_H} - \frac{Q_{c2}}{T_m}\right) \quad (35)$$

Since  $Q_{c2} = Q_{H1}$ , the total irreversibility can be calculated as follows:

$$Irr = Irr_1 + Irr_2 = T_0 \left(\frac{Q_{H2}}{T_H} - \frac{Q_{c1}}{T_c}\right) \quad (36)$$

$$\text{power} = P_1 + P_2 = Q_{H2} - Q_{c1} \quad (37)$$

Where  $\left(\frac{Q_{H2}}{T_H} - \frac{Q_{c1}}{T_c}\right)$  is entropy generation rate ( $S_{gen}$ ),  $T_0$  is environment temperature, in this study ,the environment temperature  $T_0$  is 298.15 K, hence  $Irr$  can be expressed as:

$$Irr = T_0 S_{gen} \quad (38)$$

After replacing  $Q_{H2}$ ,  $Q_{c1}$  in the equation,  $Irr$  can be expressed as (when  $m = 1$ ,  $n =$

2):

$$Irr = T_0 \left[ \frac{\alpha I(2T_2T_C - T_1T_H)}{T_H T_C} + \frac{I^2 R(2T_C + T_H)}{2T_H T_C} + \frac{K[2(T_m - T_2)T_C + (T_m - T_1)T_H]}{T_H T_C} - \frac{\tau I[2(T_2 - T_m)T_C + T_H(T_m - T_1)]}{2T_H T_C} \right] \quad (39)$$

The exergy efficiency of the two-stage TEC system can be expressed as follows, since when wind speed keeps constant, the value of  $P_{fan}$  keeps invariable, so COP is proportional to exergy efficiency.

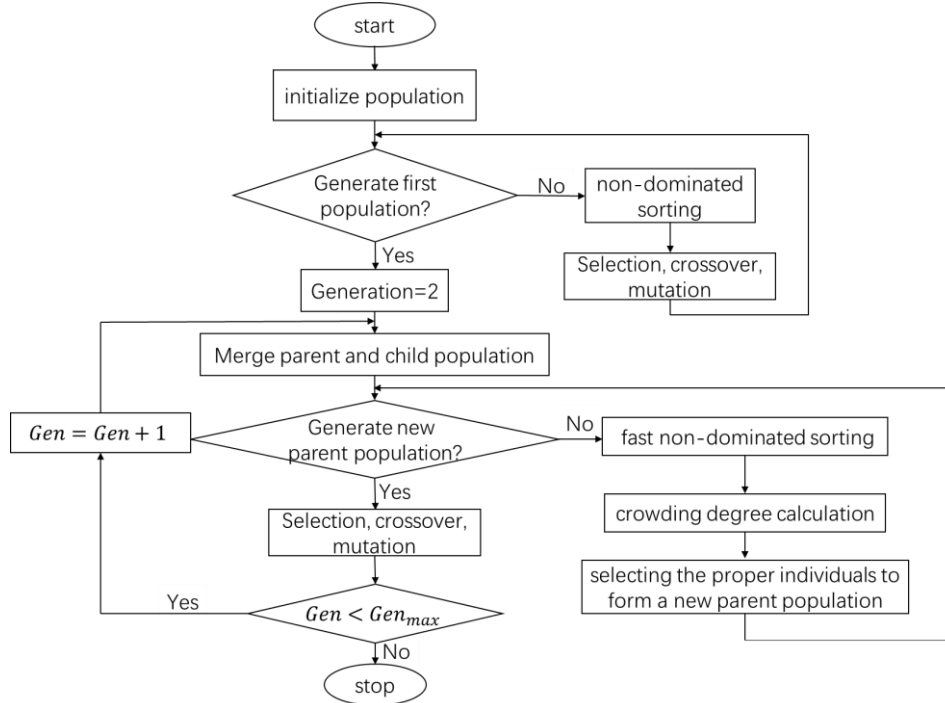
$$\eta_{ex} = \frac{Q_c \times \left(\frac{T_0}{T_c} - 1\right)}{(Power + P_{fan})} \quad (40)$$

#### 4. Optimization Procedure

NSGA-II is based on genetic algorithm; the basic idea of NSGA-II is as follows: First, randomly generate an initial population of size N, after the non-dominated sorting; the first generation of the progeny population is obtained through the three basic operations of selection, crossover and mutation of the genetic algorithm. Secondly, starting from the second generation, the parent population is merged with the child population to perform fast non-dominated sorting, and the crowding degree is calculated for each individual in the non-dominated layer, select appropriate individuals to form a new parent population based on non-dominated relationships and individual crowding; Finally, a new progeny population is generated by genetic algorithm, conduct in the similar way, until the ending condition is satisfied. The corresponding program flow chart is shown in Fig.4.

In multi-objective planning, because of conflicts between objectives, and incomparable conditions which means that one solution is best on one objective and may be poor on other objectives. Non-dominated set (Pareto set) was proposed, which defined as: Suppose that for any two solutions S1 and S2, S1 always superior to S2, then we call S1 dominates over S2. If the solution of S1 is not dominated by other solutions, then S1 is called non-dominated solution (Pareto solution), it refers to an ideal state of resource allocation. The set of the non-dominated solutions is called Pareto Front. These non-dominated solutions have the least objective conflicts

1 compared to other solutions, providing a better choice for decision makers. This  
 2 optimization method has been applied to the geometric optimization of many devices  
 3 [32-35].  
 4  
 5  
 6



31 Fig. 4. Flow chart of NSGA-II.

32  
 33  
 34 **4.1. Objective function**

35 Two incompatible objective functions are considered in this study, which are  
 36 defined as follows:  
 37

$$38 \quad J_1 = -\eta_{ex} \text{ and } J_2 = Irr \quad (41)$$

39  
 40 Where  $\eta_{ex}$  is exergy efficiency in Eq. (40), since the default of genetic algorithm is  
 41 to seek for minimum value, so in order to obtain the maximum exergy efficiency,  $J_1$   
 42 should be a negative value of exergy efficiency.  $Irr$  is irreversibility which shown in  
 43 Eq. (36). So, a two-stage TEC with small irreversibility and high exergy efficiency  
 44 can be obtained when two objective functions reach to their minimum.  
 45  
 46  
 47  
 48  
 49  
 50  
 51

52  
 53 **4.2. Constraint condition**

54 Three variables to be optimized and their upper and lower constraints are set:  
 55

$$56 \quad 0.3 A < I < 9 A$$

$$57 \quad 0.4 < \gamma < 2.5$$

$$0.8 \text{ mm} < H_L < 2.5 \text{ mm}$$

With the exception of the above constraints, some extreme situations are not desirable, such as a negative COP value, which should be eliminated in the optimization process. The population size and number of generation are 20 and 50, respectively, and 0.7 is selected as the Pareto fraction.

## 5. Decision making methods

In order to select a most desirable point in Pareto set, some decision methods are employed in the process. Three methods, TOPSIS, Shannon entropy and LINMAP, are discussed and compared in this study.

### 5.1. TOPSIS

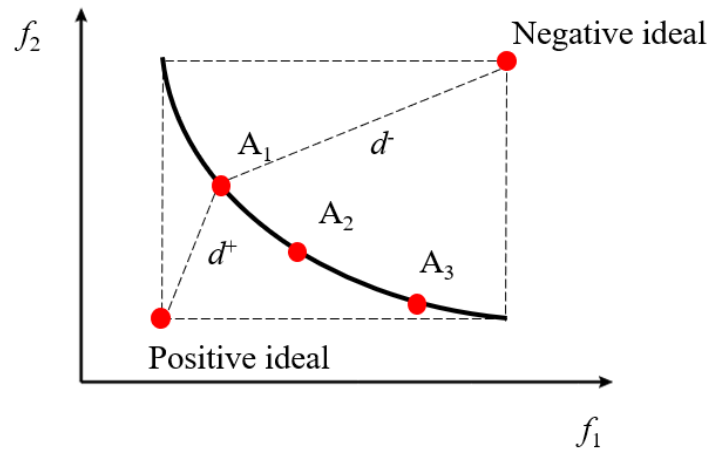


Fig. 5. The principle of TOPSIS decision making method.

TOPSIS (Technique for Order Preference by Similarity to an Ideal Solution) is a compromise method for multi-objective decision analysis of limited schemes in systems engineering [36]. The principle of the compromise solution is to seek a relatively satisfactory solution between the positive ideal solution and the negative ideal solution. Although the positive ideal solution and negative ideal solution may not exist, but they are good reference standard to measure the quality of a feasible solution. The priority solution of the decision should be as close as possible to the positive ideal solution or as far as possible from the negative ideal solution. The basic idea is shown as Fig.5.



To deal with the data matrix in the same trends (to transfer the high optimal index  $X_{ij}$  into low optimal index  $X'_{ij}$ ) and normalization, find out the best and worst solutions in the limited solution, which are positive ideal point and negative ideal point in the Fig. 5, calculate the distance between every pareto points and the best solution ( $d^+$ ) and the worst solution ( $d^-$ ) separately. Obtain the relative proximity ( $C_i$ ) of each pareto point to the positive ideal point as a basis for evaluating the good or bad.

The co-trend process:

$$X'_{ij} = 1/X_{ij} \quad (42)$$

The normalization process:

$$a_{ij} = \frac{x'_{ij}}{\sqrt{\sum_{i=1}^n (x'_{ij})^2}} \quad (43)$$

Obtain the relative proximity:

$$C_i = \frac{d_i^-}{d_i^+ + d_i^-}, i = 1, 2, \dots, m \quad (44)$$

For the point with maximal C is the most desirable point.

## 5.2. Shannon's entropy method

Shannon's entropy method is employed to obtain the weight coefficient of each objective [37-38]. Given that  $n$  alternatives and  $m$  objectives are in decision matrix  $M_{ij}$ , the process of the Shannon's entropy method is as follows.

$L_{ij}$  is the contribution rate of the  $i^{\text{th}}$  alternative in the  $j^{\text{th}}$  objective:

$$L_{ij} = \frac{F_{ij}}{\sum_{i=1}^n F_{ij}}, \quad i = 1, 2, \dots, n, j = 1, 2, \dots, m \quad (45)$$

$E_{ij}$  is the total contribution of all alternatives:

$$E_j = -K \sum_{i=1}^m P_{ij} \ln(P_{ij}) \quad (46)$$

Where  $K = 1/\ln(m)$ , deviation degree  $D_j$  is:

$$D_j = 1 - E_j \quad (47)$$

The weight coefficient  $W_j$  of the  $j^{\text{th}}$  objective is:

$$W_j = \frac{D_j}{\sum_{i=1}^m D_j} \quad (48)$$

1  
2  
3  
4  
5  
6  
7  
8  
9  
10  
11  
12  
13  
14  
15  
16  
17  
18  
19  
20  
21  
22  
23  
24  
25  
26  
27  
28  
29  
30  
31  
32  
33  
34  
35  
36  
37  
38  
39  
40  
41  
42  
43  
44  
45  
46  
47  
48  
49  
50  
51  
52  
53  
54  
55  
56  
57  
58  
59  
60  
61  
62  
63  
64  
65

Ultimately,

$$R_i = L_{ij}W_j \quad (49)$$

The Shannon's entropy method calculates each point of the Pareto front, where the point with the maximum  $R_i$  is the desirable solution.

### 5.3. LINMAP method

LINMAP decision making method is based on the Euclidian non-dimensionalization. In this method, a non-dimensionalized objective both in maximizing and minimizing is defined as follows:

$$F_{ij}^n = \frac{F_{ij}}{\sqrt{\sum_{i=1}^m F_{ij}^2}} \quad (50)$$

It is clearly known that the positive ideal point in Pareto Front is impossible to reach, because of the conflict objectives in NSGA-II. For instance, in dual objective optimization, one objective reaches to its optimal condition while the other objective reaches to its worst. After Euclidian non-dimensionalization of all objectives, the special distance of each point on the Pareto Front can be expressed as follows:

$$d_i^+ = \sqrt{\sum_{j=1}^n (F_{ij} - F_j^{Ideal})^2} \quad (51)$$

Where  $i$  is each point on the Pareto Front and  $n$  is the number of the objective. And  $F_j^{Ideal}$  is the ideal solution of each objective. LINMAP approach computes the point on Pareto frontier with minimum distance from the ideal solution.

And also, decision makers can also choose the points on both ends of the line, based on their criteria for higher exergy efficiency or lower Irreversible losses.

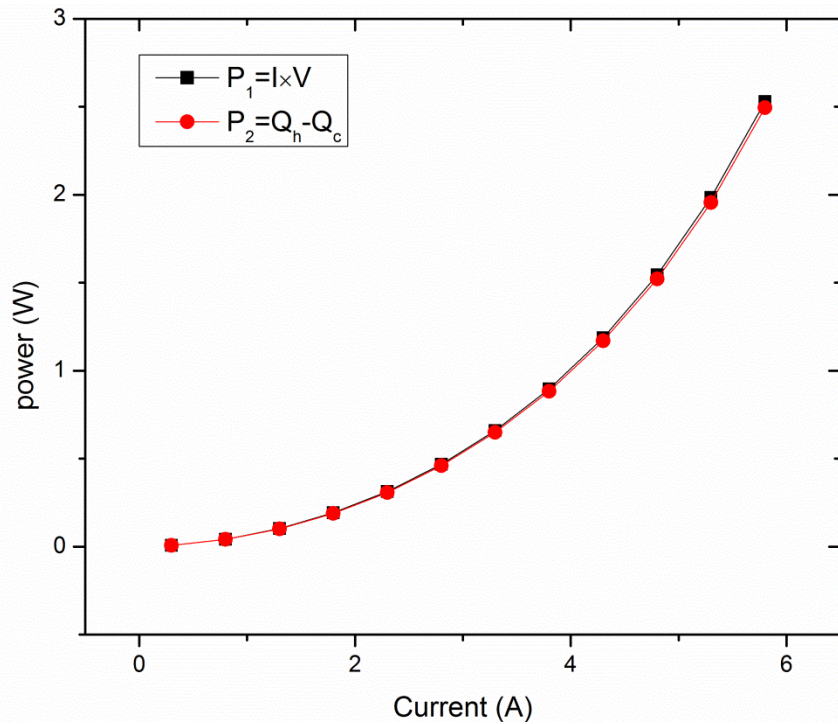
## 6. Results and discussion

### 6.1. Model validation

Both electric field and temperature field are coupled in the TEC model. To validate self-consistency of the model, power consumption can be calculated in both versions. Power consumption can be expressed as  $P_1 = I \times V$ , and also  $P_2 = Q_{H2} - Q_{C1}$ . The comparison for two calculating methods is shown in Fig.6, the maximum relative

1 deviation  $(P_2 - P_1)/P_1$  is -1.6%, which indicates that the present model has  
2 self-consistency.  
3

4 To validate the TEC model, a comparison with the result in literature [26] is carried  
5 out to validate the simulation model. The physical property parameters of  $\text{Bi}_2\text{Te}_3$  are  
6 modified based on literature [39], the boundary condition is modified, where the hot  
7 side temperature is 300 K, and cold side temperature is 280 K, the number of TE legs  
8 on colder stage and hotter stage are 10 and 20, respectively. The heat conductivity of  
9 lower and upper substrate is assumed to be infinity. As shown in Fig.7, the relative  
10 deviation between present model and Literature [26] is less than 4%.  
11  
12  
13  
14  
15  
16  
17  
18  
19  
20



21  
22  
23  
24  
25  
26  
27  
28  
29  
30  
31  
32  
33  
34  
35  
36  
37  
38  
39  
40  
41  
42  
43  
44  
45 Fig. 6. Power consumption at various currents for two-stage series-connected TEC model.  
46  
47  
48  
49  
50  
51  
52  
53  
54  
55  
56  
57  
58  
59  
60  
61  
62  
63  
64  
65

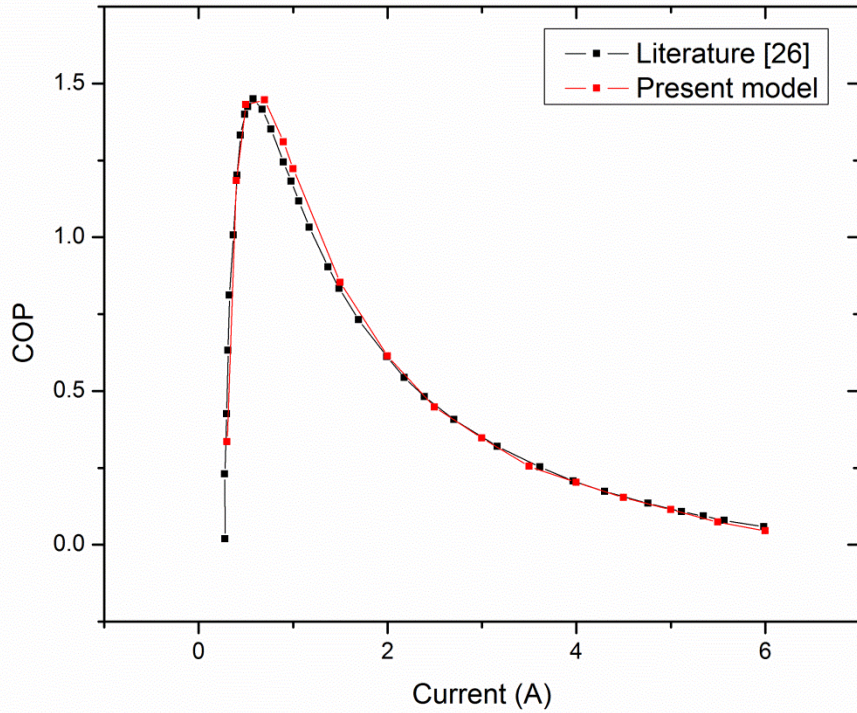


Fig. 7. Comparison of present model with result in literature [26].

## 6.2. Single factor sensitivity analysis

To validate the effect of variables to be optimized on the performance of TEC system both in series and parallel connection, single factor sensitivity analysis is employed, and the initial value of variables to be optimized are shown in Table 4.

Table 4 Initial value of variables to be optimized

Variables	Symbol	Value	Unit
Electrical current	$I$	2	A
Ratio of channel width to thickness of fin	$\gamma$	1.5	1
Height of lower stage TE legs	$H_L$	1.6	mm

Three parameters studied in this paper, electric current ( $I$ ), ratio of channel width to thickness of fin ( $\gamma$ ), and height of lower stage TE legs ( $H_L$ ). Fig.8 shows how electrical current effects on the performance of TEC both in series and parallel

connection.

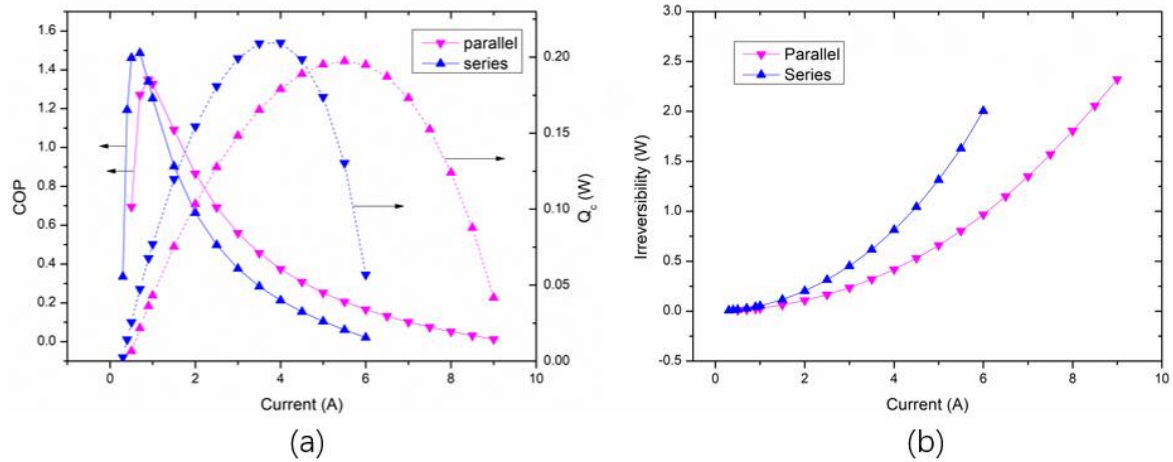


Fig. 8. Variation of (a) COP and  $Q_c$  and (b) Irreversibility with electric current in both parallel connection and series connection.

Fig. 8(a) shows that as the electrical current increases, COP first increases rapidly then decreases slowly. In the same time,  $Q_c$  first increases to the maximum point with the increases of electrical current then decreases. We can notice that for both series and parallel connection TEC model, COP and  $Q_c$  cannot reach to their maximum point simultaneously. Compared with parallel connection TEC, a higher electrical current (6 A ~ 9 A) may cause a negative cooling power and COP in series connection TEC model. This is mainly because that the Joule heat generated by the larger current is more than the cooling capacity; this case is undesirable in the study.

Fig. 8(b) shows that irreversibility increases with increase of the electrical current, and at the same electrical current, the irreversibility of series connection TEC model is higher than that of parallel connection TEC model when other boundary conditions are fixed. In general, a relative small electrical current may lead to a high COP and low irreversibility, while a relative high electrical current may lead to a high cooling power but low efficiency and greater irreversibility.

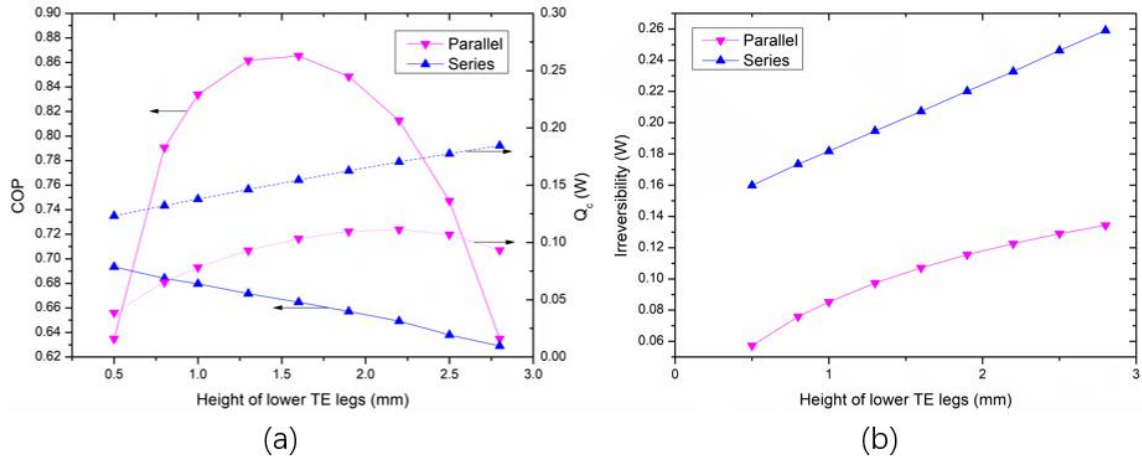


Fig. 9. Variation of (a) COP and  $Q_c$  and (b) Irreversibility with height of lower TE legs in both parallel connection and series connection.

Fig. 9 shows how COP,  $Q_c$  and irreversibility change with the height of lower TE legs in both parallel and series connection TEC model. In series connection, COP decreases with increases of  $H_L$ , while  $Q_c$  and irreversibility increase with increases of  $H_L$ . In parallel connection, COP and  $Q_c$  first increase then decrease with increases of  $H_L$ , but they do not reach to their maximum point simultaneously. The irreversibility increases with the increases of height of lower TE legs.

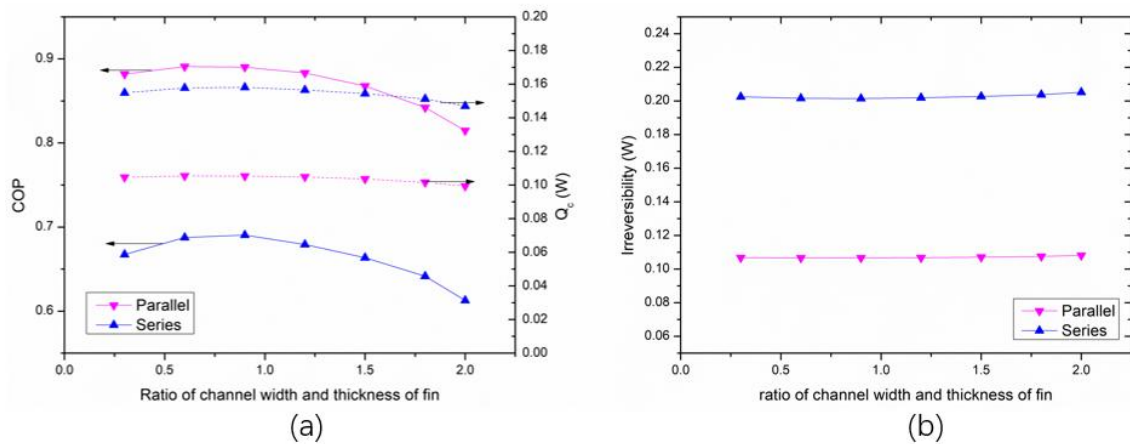


Fig. 10. Variation of (a) COP and  $Q_c$  and (b) Irreversibility with ratio of channel width to thickness of fin in both parallel connection and series connection.

Fig. 10 indicates the relationship between ratio of channel width to thickness of fin and COP,  $Q_c$ , and irreversibility. We can clearly see that COP first slowly increases

and then decreases both in parallel and series connection. But the ratio of channel width and thickness of fin shows little influence on  $Q_c$  and irreversibility.

### 6.3. Optimization Results

The Pareto fronts obtained by NSGA-II for Series-connected TEC and Parallel-connected TEC are shown as Fig. 11 and Fig. 12. The Ideal and Nadir solution for two-objective optimization of Series-connected TEC model are (-0.10178, 0.006828 W) (-0.03956, 0.018055 W), respectively. And the Ideal and Nadir solution for two-objective optimization of Parallel-connected TEC model are (-0.12534, 0.007545 W) (-0.02745, 0.022301 W), respectively. To identify the relative position to Ideal solution and Nadir solution of points obtained by three decision making methods, the deviation index can be calculated as follows:

$$d = \frac{d^+}{d^+ + d^-} \quad (52)$$

Where  $d^+$  is the distance to Ideal solution and  $d^-$  is the distance to Nadir solution, which can be written as follows:

$$d^+ = \sqrt{\sum_{j=1}^n (F_j - F_j^{Ideal})^2} \quad (53)$$

$$d^- = \sqrt{\sum_{j=1}^n (F_j - F_j^{Nadir})^2} \quad (54)$$

The Ideal solution and Nadir solution reveal the best condition and the worst condition, which may not achievable. The deviation index ranges from 0 to 1. The closer the points on the Pareto front to the Ideal solution, the closer the value of deviation index to 0.

Fig.13 shows the deviation index of three decision making methods for both parallel and series connected TEC models and Table 5 shows the comparison of three decision making methods. It can be clearly seen that among three decision making methods, LINMAP achieves the minimum deviation index, which means that the optimal solution selected by LINMAP is the most desirable solution among them, and the value of exergy efficiency and Irreversibility are closest to the Ideal ones. The optimal solution selected by LINMAP of Series and Parallel connected TEC models are (-0.0964, 0.01282 W), (-0.1143, 0.0152 W), respectively. And the optimized

variables chosen by LINMAP are shown in Table 6.

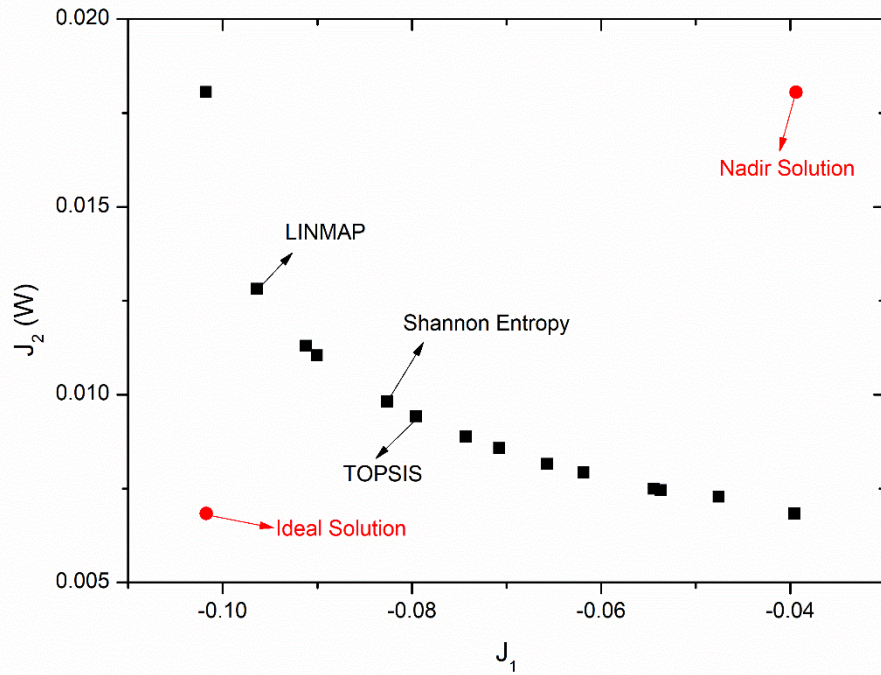


Fig.11. Pareto front for two objectives optimization of Series-connected TEC model.

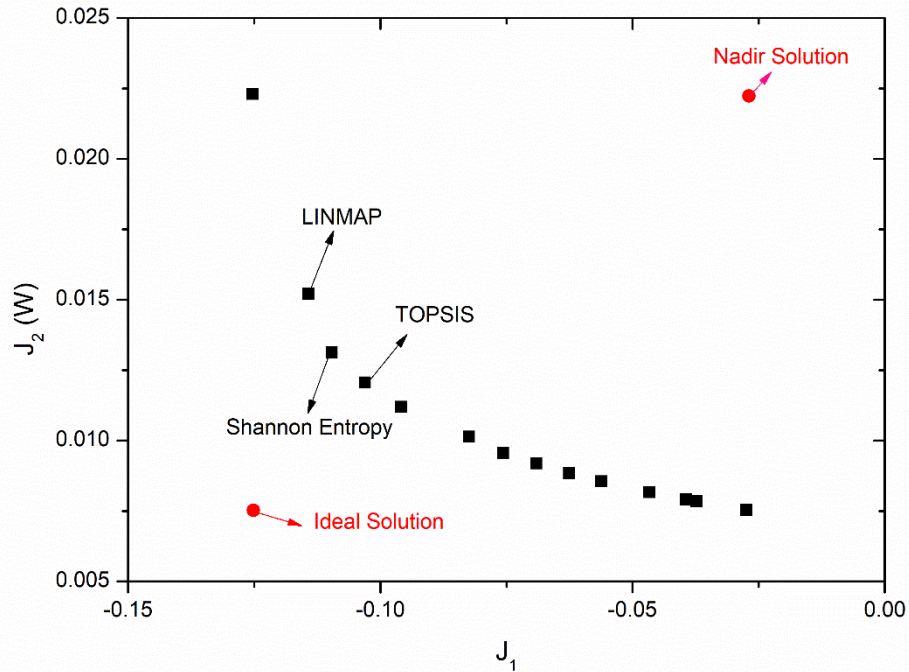


Fig.12. Pareto front for two objectives optimization of Parallel-connected TEC model.



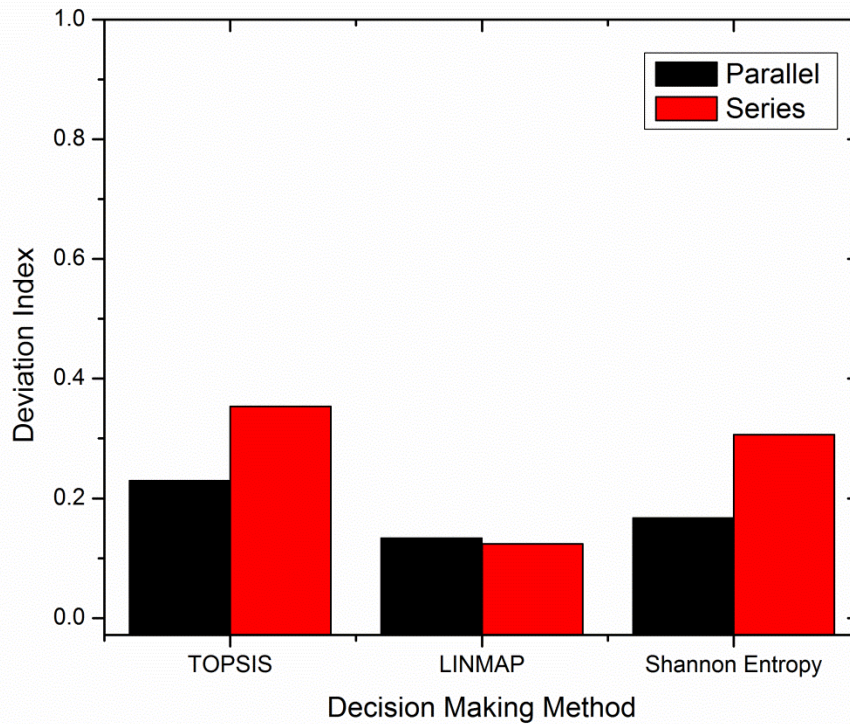


Fig. 13. Deviation Index of three decision making method for both Series and Parallel connected TEC models.

Table 5 Comparison between optimal solutions using three decision making methods for both Series and Parallel connected TEC models

Optimization algorithm	Decision making method	Series		Parallel	
		J1	J2	J1	J2
		(-)	(W)	(-)	(W)
NSGA-II	TOPSIS	-0.0796	0.00943	-0.1031	0.01205
	LINMAP (best)	<b>-0.0964</b>	<b>0.01282</b>	<b>-0.1143</b>	<b>0.0152</b>
	Shannon Entropy	-0.0826	0.00981	-0.1097	0.01313
Ideal solution		-0.1018	0.00683	-0.1253	0.00754
Nadir solution		-0.0396	0.01806	-0.0274	0.0223

Table 6 The optimized variables chosen by LINMAP decision making method

LINMAP	$I$ (A)	$H_L$ (mm)	$\gamma$
Parallel	0.65	1.882	0.701
Series	0.46	1.448	0.772

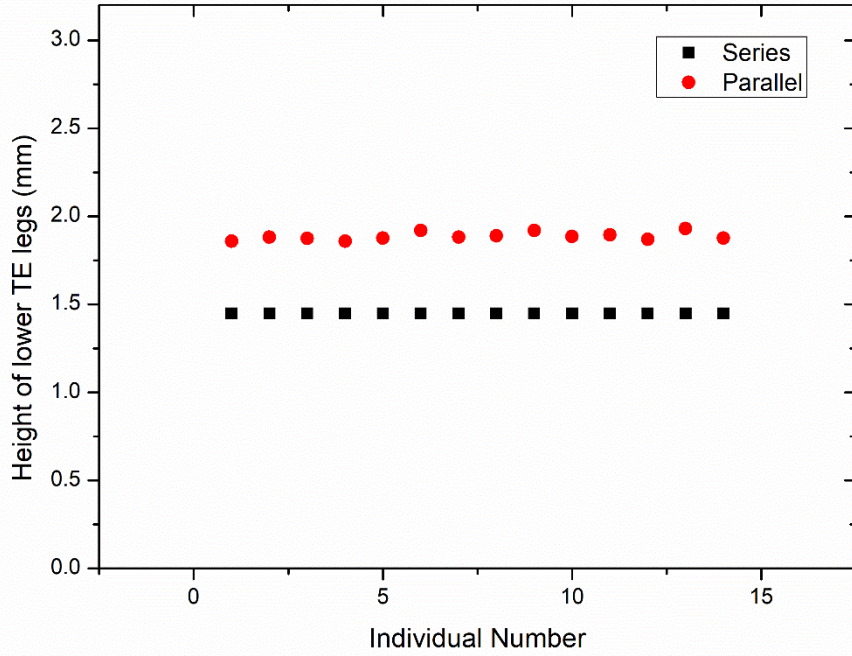
Fig. 14 to Fig. 16 show the influence of three optimized geometric parameters on performance of Series and Parallel connected TEC model along with the Pareto front.

1 It can be clearly seen in Fig. 14 that the overwhelming majority values of  $H_L$  of Series  
2 TEC are around 1.45 mm while those of Parallel TEC are around 1.89 mm,  
3 respectively. It indicates that, for a two-stage TEC with constant volume, there is an  
4 optimal ratio between the upper stage and lower stage height to achieve the highest  
5 exergy efficiency. To determine the optimal electrical current is also significant in  
6 practical application, it can be clearly seen in Fig. 15 that with the electrical current  
7 increases from 0.31 A to 0.56 A in Series and 0.41 A to 0.81 A in Parallel, the exergy  
8 efficiency and irreversibility increase simultaneously, since COP is proportional to  
9 exergy efficiency, the COP increase as well. It indicates that a higher current increases  
10 the performance of the model while increasing the irreversible loss of the model. Fig.  
11 16 shows the influence of  $\gamma$  on the TEC's performance. It can be seen that with  
12 increase of the exergy efficiency and irreversibility, the individual point desultorily  
13 distributes in a range of (0.55,1.2), this result also confirms the results shown in  
14 Fig.10, that  $\gamma$  shows a little influence on  $Q_c$  and irreversibility and COP first slowly  
15 increase and then decrease both in parallel and series connection. Since COP is  
16 proportional to exergy efficiency, the trend of exergy efficiency with  $\gamma$  is the same as  
17 that of COP.

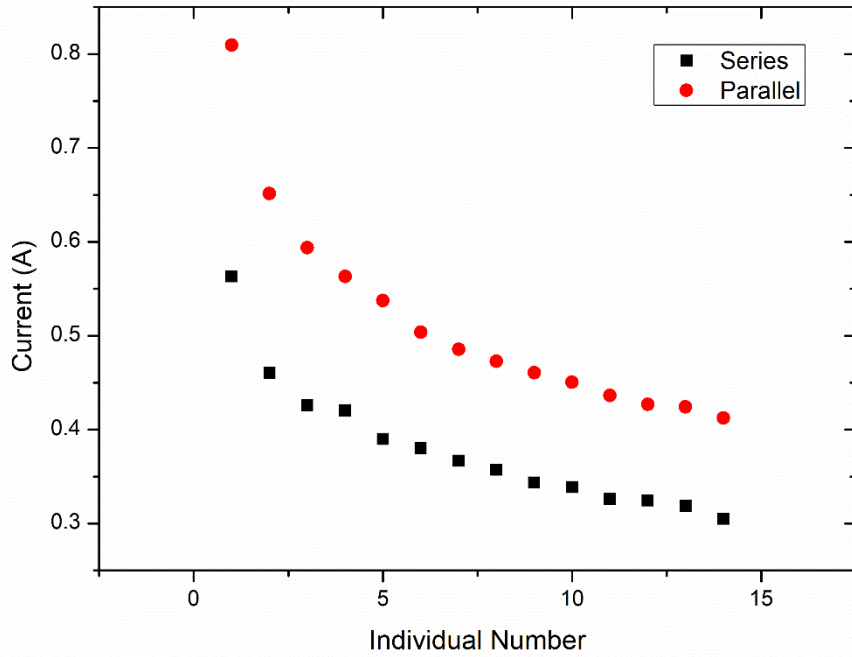
18 It is worth noting that when the required temperature difference is the same as  
19 that of the series type, the parallel type of power consumption is less, and with the  
20 electrical current increases from 0.5 A to 6 A, the power consumption saved by  
21 parallel type than series type increase from 45.5% to 56.2%, which is shown in Fig.  
22 17, and since there is no intermediate substrate, the inter-stage temperature difference  
23 is reduced. But the circuit design of parallel type is much more complicated than that  
24 of series type especially the TEC is more than two stages.

25 To illustrate the effectiveness of fin heat exchanger to performance of TEC, the  
26 comparison of COP between TEC with and without plate-fin exchanger is conducted  
27 in Fig. 18, it shows the trend of COP with electrical current in two-stage series TEC  
28 model and two-stage parallel TEC model, two curves (with and without fin) change in  
29 the same trend, and both increase sharply and then decrease. On average, the COP of  
30 series TEC with fin is approximately 1.48 times larger than the series TEC without fin

1 while for parallel TEC the value of which is 1.84. On the other hand, adding fin at the  
2 hot side greatly improves the performance of TEC.  
3



31 Fig. 14. Variation of optimal height of lower TE legs.



60 Fig. 15. Variation of optimal electrical current.

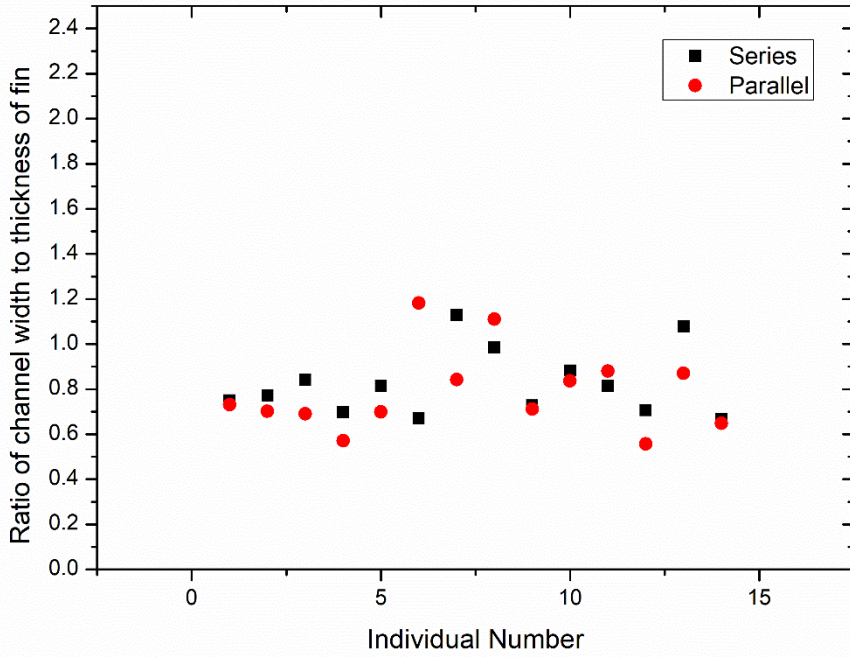


Fig. 16. Variation of optimal ratio of channel width to thickness of fin.

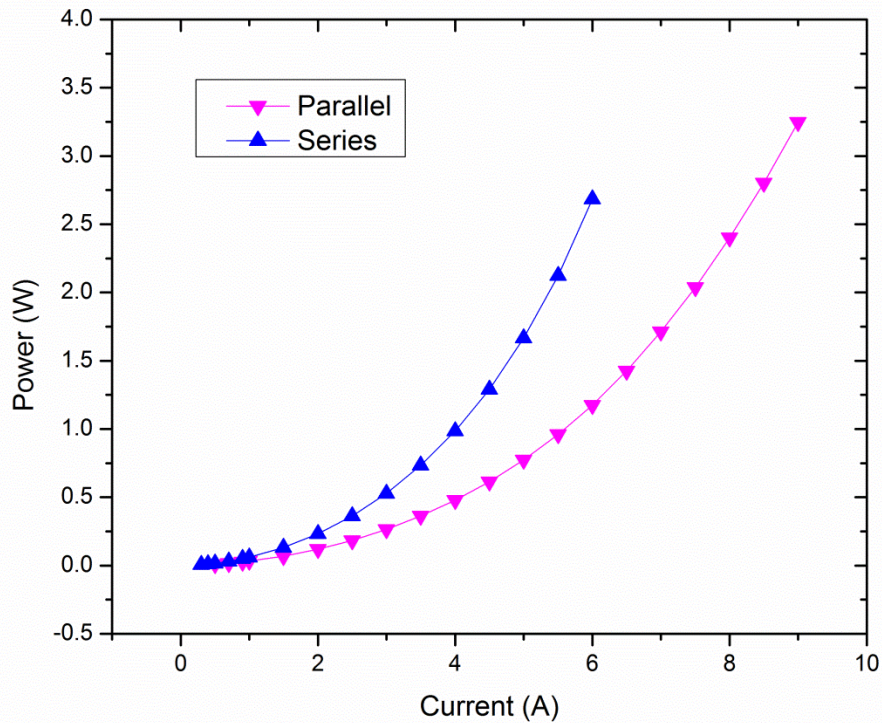
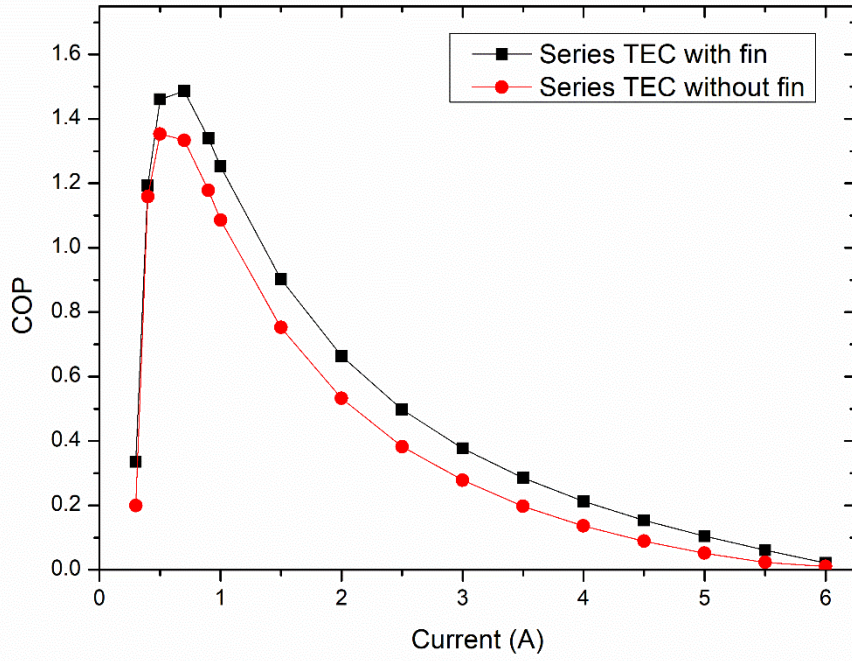
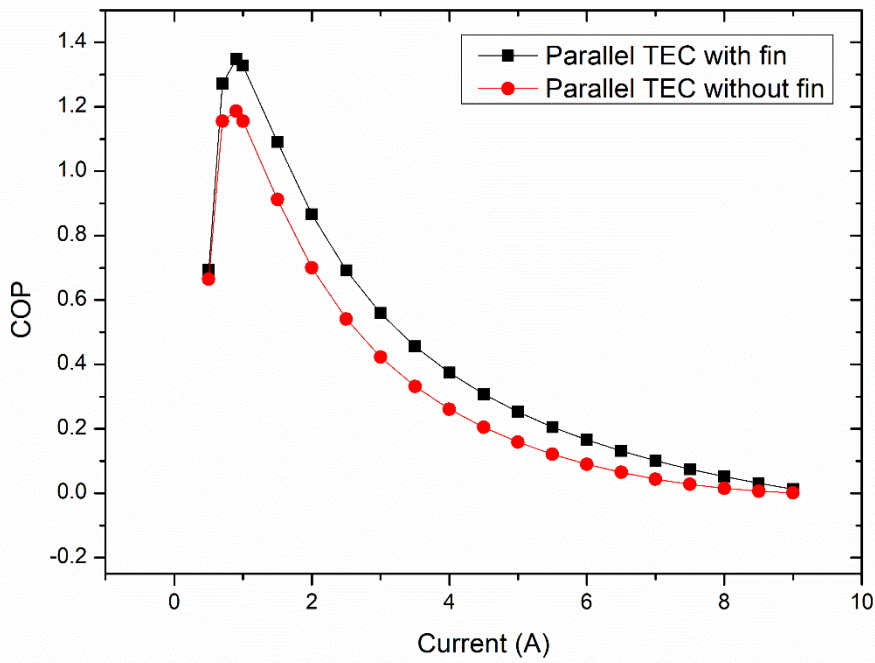


Fig. 17. The power consumption of series-connected TEC and parallel-connected TEC varies with current.



(a)



(b)

Fig. 18. COP vary along electric current in (a) two-stage series TEC (b) two-stage parallel TEC ( $\gamma = 1.5, H_L = 1.6mm$ ).

## 7. Conclusion

The parallel- and series-connected two-stage TEC with fin has been compared. Exergy efficiency and irreversibility have been optimized by NSGA-II simultaneously. Pareto solutions of two models are obtained and the most compromised solution in the Pareto solutions is chosen. The main conclusions shown as follows:

- (1) The solution selected by LINMAP is the most compromising solutions.
- (2) For a two stage TEC model (both in parallel and series connected) there exists an optimal ratio of TE legs between the upper stage and the lower stage to provide maximum exergy efficiency (as well as COP) and minimum irreversibility when the total volume of thermoelectric material is fixed. A higher current increases the exergy efficiency (as well as COP) of the model while increasing the irreversible loss of the model.
- (3) TEC model with plate-fin heat exchanger have better performance both in parallel and series connected than TEC without fin. But the ratio of channel width and thickness of fin has some influence on COP while shows little influence on  $Q_c$  and irreversibility.
- (4) When the required temperature difference is the same, the parallel connected TEC saves about 50% of the power consumption compared to the series connected TEC, but the circuit design of parallel type is more complicated than that of series type, especially the TEC is more than two stages.

## Nomenclature

$ZT$	figure of merit
$T$	temperature (K)
$T_0$	environment temperature (K)
$T_1$	temperature at the cold junction of TEC (K)
$T_2$	temperature at the hot junction of TEC (K)
$T_m$	temperature of the middle substrate (K)
$T_C$	temperature at the cold side (K)

1	$T_H$	temperature at the hot side (K)
2	$R$	electrical resistance ( $\Omega$ )
3		
4	$H_L$	height of lower stage TE legs (mm)
5		
6	$H$	length of fin (mm)
7		
8	$\gamma$	Ratio of channel width to thickness of fin
9		
10	$N$	Number of the fin (integer)
11		
12	$\eta_{ex}$	Exergy efficiency
13		
14	$J$	objective function
15		
16	$I$	electrical current (A)
17		
18	$T_f'$	Inlet temperature of channel (K)
19		
20	$T_f''$	outlet temperature of channel (K)
21		
22	$K$	heat conductance of the thermoelectric pairs (W/K)
23		
24		
25		
26		
27	<i>Greek letters</i>	
28		
29	$\alpha$	Seebeck coefficient (V/K)
30		
31	$\lambda$	thermal conductivity (W/m·K)
32		
33	$\sigma$	electrical conductivity (S/m)
34		
35	$\tau$	Thomson coefficient
36		
37	<i>Subscript</i>	
38		
39	1	upper stage
40		
41	2	lower stage
42		
43	ex	exergy
44		
45	C	cold side
46		
47	H	hot side
48		
49	<i>Acronyms and abbreviations</i>	
50		
51	TEC	thermoelectric cooler
52		
53	TEG	thermoelectric generator
54		
55	NSGA-II	non-dominated Sorting Genetic Algorithm
56		
57	COP	coefficient of performance
58		
59	TOPSIS	Technique for Order Preference by Similarity to an Ideal Solution
60		
61		
62		
63		
64		
65		

1  
2  
3  
4  
5  
6  
7  
8  
9  
10  
11  
12  
13  
14  
15  
16  
17  
18  
19  
20  
21  
22  
23  
24  
25  
26  
27  
28  
29  
30  
31  
32  
33  
34  
35  
36  
37  
38  
39  
40  
41  
42  
43  
44  
45  
46  
47  
48  
49  
50  
51  
52  
53  
54  
55  
56  
57  
58  
59  
60  
61  
62  
63  
64  
65

Irr                      Irreversibility (W)

### **Acknowledgment**

The work is supported by the National Natural Science Foundation of China (NOs.51776079 & 51736004) and the National Key Research and Development Program of China (NO. 2017YFB0603501-3).

Sergio Usón would like to acknowledge Universidad de Zaragoza and Fundación Ibercaja for financing the Project “Exergy analysis of Energy Conversion Systems based on Thermoelectric Materials” Reference: JIUZ-2017-TEC-10.

### **Reference**

- [1] Arash N, Hossein N, Mortaza Y, Faramarz R, Hojjatollah RK. Development of an exergoeconomic model for analysis and multi-objective optimization of a thermoelectric heat pump. *Energy Conversion and Management* 2016;130:1-13.
- [2] Ge Y, Liu ZC, Sun HN, Liu W. Optimal design of a segmented thermoelectric generator based on three-dimensional numerical simulation and multi-objective genetic algorithm. *Energy*, 2018; 147:1060–9.
- [3] Cheng YH, Chunkuan S. Maximizing the cooling capacity and COP of two-stage thermoelectric coolers through genetic algorithm. *Applied Thermal Engineering* 2006;26:937-47.
- [4] Hee SK, Keiko K. Design of segmented thermoelectric generator based on cost-effective and light-weight thermoelectric alloys. *Materials Science and Engineering B* 2014;185:45–52.
- [5] Zhao XB, Ji XH, Zhang YH. Bismuth telluride nanotubes and the effects on the thermoelectric properties of nanotube-containing nanocomposites. *Applied Physics Letters* 2005; 86(6):1665.
- [6] Poudel B, Qing H, Ren Z. High-thermoelectric performance of nanostructured



1 bismuth antimony telluride bulk alloys. *Science* 2008;320(5876):634–8.

2 [7] Hu LP, Zhu TJ, Liu XH, Zhao X. Point defect engineering of high-performance  
3 bismuth-telluride-based thermoelectric materials. *Advanced Functional Materials*  
4 2014; 24(33): 5211–8.  
5  
6

7 [8] Biswas K, He J, Blum ID. High-performance bulk thermoelectrics with all-scale  
8 hierarchical architectures. *Nature* 2012;489(7416):414–8.  
9

10 [9] Wang Y, Rogado NS, Cava RJ. Spin entropy as the likely source of enhanced  
11 thermopower in  $\text{Na}_x\text{Co}_2\text{O}_4$ . *Nature* 2003; 423(6938):425–8.  
12

13 [10] Hu Y, Zeng L, Minnich AJ, Dresselhaus MS, Chen G. Spectral mapping of  
14 thermal conductivity through nanoscale ballistic transport. *Nature Nanotechnology*  
15 2015;10:701–6.  
16

17 [11] Zeng L, Chen G. Disparate quasiballistic heat conduction regimes from periodic  
18 heat sources on a substrate. *Applied Physics* 2014;116(6): 539.  
19

20 [12] Amin H. Optimization of electrically separated two-stage thermoelectric  
21 refrigeration systems using chemical reaction optimization algorithm. *Applied*  
22 *Thermal Engineering*.2017;123:514-26.  
23

24 [13] Ravita L, Kaushik SC, Tyagi SK. Geometric optimization of trapezoidal  
25 thermoelectric heat pump considering contact resistances through genetic algorithm.  
26 *International Journal of Energy Research* 2018;42:633-47.  
27

28 [14] Pablo E, Miguel A. Analysis of a Hybrid Thermoelectric Microcooler: Thomson  
29 Heat and Geometric Optimization. *Entropy* 2017;19:312-29.  
30

31 [15] Chen YH, Lin WK. Geometric optimization of thermoelectric coolers in a  
32 confined volume using genetic algorithms. *Applied Thermal Engineering*  
33 2005;25:2983-97.  
34

35 [16] Cheng YH, Chunkuan S. Maximizing the cooling capacity and COP of two-stage  
36 thermoelectric coolers through genetic algorithm. *Applied Thermal Engineering*  
37 2006;26:937-47  
38

39 [17] Chen JH, Yu JL, Ma M. Theoretical study on an integrated two-stage cascaded  
40 thermoelectric module operating with dual power sources. *Energy Conversion and*  
41 *Management* 2015;98:28-33.  
42  
43  
44  
45  
46  
47  
48  
49  
50  
51  
52  
53  
54  
55  
56  
57  
58  
59  
60  
61  
62  
63  
64  
65

- 1 [18] Sharma S, Dwivedi VK, Pandit SN. Exergy analysis of single-stage and multi  
2 stage thermoelectric cooler. *International Journal of Energy Research* 2014;38:213-22.  
3  
4 [19] Simak J, Mortaza Y, Farzad M. Performance improvement of a transcritical CO<sub>2</sub>  
5 refrigeration cycle using two-stage thermoelectric modules in sub-cooler and gas  
6 cooler. *International Journal of Refrigeration*. 2017;74:105.  
7  
8 [20] Ranjana A, Rajesh A. Multiobjective optimization and analytical comparison of  
9 single - and 2 - stage (series/parallel) thermoelectric heat pumps. *International*  
10 *Journal of Energy Research* 2018;42:1760-78.  
11  
12 [21] Zhu L, Yu JL. Optimization of heat sink of thermoelectric cooler using entropy  
13 generation analysis. *International Journal of Thermal Sciences* 2017;118:168-175.  
14  
15 [22] Meng F, Chen L, Sun F. Performance Prediction and Irreversibility Analysis of a  
16 Thermoelectric Refrigerator with Finned Heat Exchanger. *ACTA PHYSICA*  
17 *POLONICA A* 2011;120:397-406.  
18  
19 [23] Manikandan S, Kaushik SC, Anusuya K. Thermodynamic Modelling and Analysis  
20 of Thermoelectric Cooling System. 2016 International Conference on Energy  
21 Efficient Technologies for Sustainability.  
22  
23 [24] Kaushik S.C, Manikandan S, Hans R. Energy and exergy analysis of  
24 thermoelectric heat pump system. *International Journal of Heat and Mass Transfer*  
25 2015;86:843-52.  
26  
27 [25] Manikandan S, Kaushik S.C. Energy and exergy analysis of an annular  
28 thermoelectric cooler. *Energy Conversion and Management* 2015;106: 804-14.  
29  
30 [26] Kaushik SC, Manikandan S. The influence of Thomson effect in the performance  
31 optimization of a two stage thermoelectric cooler. *Cryogenics* 2015;72:57-64.  
32  
33 [27] Arash N, Hossein N, Mortaza Y, Faramarz R. Effect of geometry and applied  
34 currents on the exergy and exergoeconomic performance of a two-stage cascaded  
35 thermoelectric cooler. *International journal of refrigeration* 2018;85:1-12.  
36  
37 [28] Zhao YL, Wang SX, Ge MH, Li YZ, Yang YR. Energy and exergy analysis of  
38 thermoelectric generator system with humidified flue gas. *Energy Conversion and*  
39 *Management* 2018;156:140-9.  
40  
41 [29] Tan HB, Fu H, Yu JL. Evaluating optimal cooling temperature of a single-stage  
42  
43  
44  
45  
46  
47  
48  
49  
50  
51  
52  
53  
54  
55  
56  
57  
58  
59  
60  
61  
62  
63  
64  
65

1 thermoelectric cooler using thermodynamic second law. Applied Thermal Engineering  
2 2017;123:845-51.  
3

4 [30] Ohare BY, Lee H. Exergetic analysis of a solar thermoelectric generator. Energy  
5 2015;91:84-90.  
6

7 [31] Arash N, Hossein N, Mortaza Y, Faramarz R, Hojjatollah RK. Development of an  
8 exergoeconomic model for analysis and multi-objective optimization of a  
9 thermoelectric heat pump. Energy Conversion and Management 2016;130:1-13.  
10

11 [32] Ge Y, Liu ZC, Liu W. Multi-objective genetic optimization of the heat transfer  
12 for tube inserted with porous media. International Journal of Heat and Mass Transfer  
13 2016;101:981-7.  
14

15 [33] Zeng XB, Ge Y, Shen J, Zeng LP, Liu ZC, Liu W. The optimization of channels  
16 for a proton exchange membrane fuel cell applying genetic algorithm. International  
17 Journal of Heat and Mass Transfer 2017;105:81-9.  
18

19 [34] Liu ZC, Zeng XB, Ge Y, Shen J, Liu W. Multi-objective optimization of  
20 operating conditions and channel structure for a proton exchange membrane fuel cell.  
21 International Journal of Heat and Mass Transfer 2017;111:289-98.  
22

23 [35] Ge Y, Liu ZC, Shan F, Yuan F, Long R, Liu W. Multi-objective arrangement  
24 optimization of a tube bundle in cross-flow using CFD and genetic algorithm. Energy  
25 procedia 2017;142:3774-9.  
26

27 [36] Huang, I.B.; Keisler, J.; Linkov, I. (2011). "Multi-criteria decision analysis in  
28 environmental science: ten years of applications and trends". Science of the Total  
29 Environment. 409: 3578–3594.  
30

31 [37] Shi YJ, Sun GH, Jing J, Dong SH. Shannon and Fisher entropy measures for a  
32 parity-restricted harmonic oscillator. Laser Physics 2017;125201.  
33

34 [38] Ranjana A, Kaushik, Rajesh A. Thermodynamic modeling and multi-objective  
35 optimization of two stage thermoelectric generator in electrically series and parallel  
36 configuration. Applied Thermal Engineering 2016; 103:1312–23.  
37

38 [39] Xuan X, Ng K, Yap C, Chua H. The maximum temperature difference and polar  
39 characteristic of two-stage thermoelectric cooler. Cryogenics 2002;42 (5):273–8.  
40  
41  
42  
43  
44  
45  
46  
47  
48  
49  
50  
51  
52  
53  
54  
55  
56  
57  
58  
59  
60  
61  
62  
63  
64  
65